JOURNAL OF MATERIALS SCIENCE 33 (1998) 3891–3898

Some considerations of asymmetric cracking in an applied-moment double cantilever beam

C. H. HSUEH, E. Y. SUN, P. F. BECHER
Metals and Ceramics Division, Oak Ridge National Laboratory, Oak Ridge, TN 37831, USA
E-mail: hsuehc@ornl.gov

J. B. LI
Department of Materials Science and Engineering, Tsinghua University, Beijing 100084, People's Republic of China

In situ observations of crack propagation in applied-moment double cantilever beam specimens have been used to obtain the *R*-curve behaviour of Si_3N_4/50% BN–50% Al_2O_3 laminated composites, in which the BN–Al_2O_3 layers function as weak interphases. The crack plane and the crack direction were, respectively, normal and parallel to the plane of the laminated layers. During crack propagation, both delamination and crack deviation from the centreline of the specimen occurred. A deviated crack resulted in an uneven moment of inertia in the two beams of the specimen. For a non-laminated material, a deviated crack would become unstable, such that the crack would propagate towards the beam with the smaller moment of inertia. It was found in the present study that delamination in a laminated composite can stabilize the propagation of a deviated crack. The stabilization of a deviated crack with delamination was due to a decrease in the inequality in the moment of inertia of the two beams compared to that without delamination.

1. Introduction

The applied-moment double cantilever beam (DCB) test has been used to characterize the fracture toughness of brittle materials [1–4]. For ceramic composites, the fracture toughness is often not a single-value parameter but can increase and asymptotically approaches a plateau value as the crack extends (i.e. the *R*-curve behaviour) [5–10]. *In situ* observations of crack propagation in an applied moment DCB specimen have been used successfully to investigate the *R*-curve behaviour of whisker-reinforced, self-reinforced, and intermetallic-bonded ceramic composites [2–4]. Recently, studies have been extended to laminated ceramic composites. However, due to the presence of weak interphases, the laminates exhibit both partial delamination and asymmetric cracking behaviour, to which the existing analyses for applied moment DCB tests cannot be readily applied. Also, compared to the propagation of a deviated crack in a non-laminated material, the propagation of a deviated crack with delamination in a laminated composite is found to be more stable during the applied moment DCB test.

The purpose of the present study was to analyse the fracture resistance of laminates exhibiting both partial delamination and asymmetric cracking during the applied moment DCB test and to address the stability problem for the propagation of a deviated crack. First, experimental observations of partial delamination and asymmetric cracking in DCB specimens of laminated ceramic composites, which contain centerline grooves to guide the crack, are presented. Then, the traditional analysis of assuming an even distribution of the applied moment between the two beams is used to analyse the fracture resistance of the composite with partial delamination and asymmetric cracking. Also, new theoretical analyses of assuming an uneven distribution of the applied moment are developed, and the criterion of minimum total elastic energy stored in the two beams during crack propagation is adopted to define the distribution of the applied moments. Finally, the stability problem of the propagation of a deviated crack with or without delamination is addressed.

2. Experimental procedure

The laminated ceramic composite used in the present study consists of alternate layers of Si_3N_4 ($\sim$68 μm thick) and 50 vol% BN–50 vol% Al_2O_3 ($\sim$30 μm thick). The average grain diameter of Si_3N_4 was 0.6 μm, and BN had platelet-shaped grains, which were oriented more or less parallel to the layer plane (Fig. 1). The processing procedures of this laminate will be reported elsewhere [11]. The DCB specimen had the dimensions 9.88 mm wide × 2.32 mm thick × 25 mm long. A 1.32 mm deep × 1.78 mm wide groove was machined at the centreline parallel to the

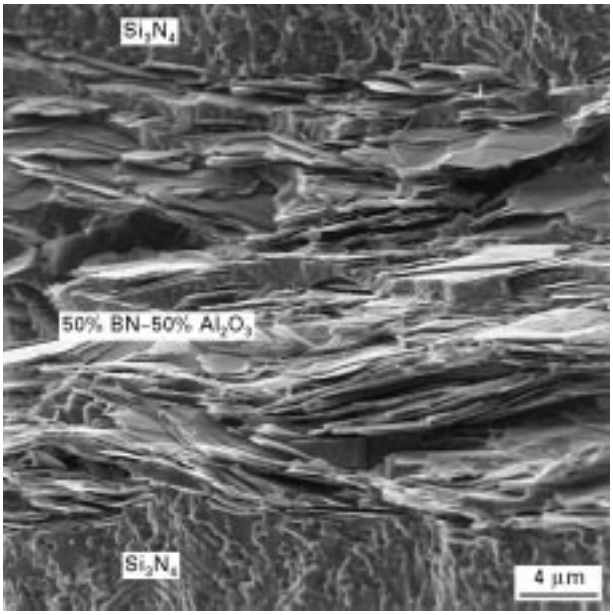

Figure 1 Scanning electron micrograph showing the cross-section of the Si_3N_4/BN–Al_2O_3 laminate.

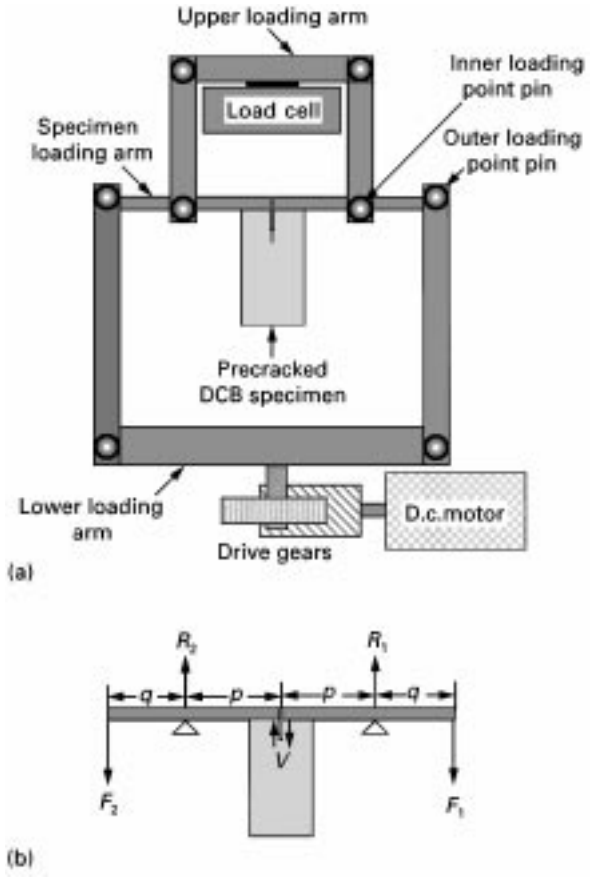

Figure 2 Schematic drawings showing (a) the loading fixture, and (b) the load on the specimen loading arm for applied-moment double cantilever beam tests.

length of the specimen on one wide surface (9.88 mm × 25 mm) to guide the crack path. The opposite surface was mechanically polished to facilitate observation of the crack. One end of the specimen was notched to form a tapered web to facilitate precracking of the specimen. An array of three to five indentations was positioned on the polished surface near the notch tip such that the radial cracks due to indentations linked in the direction parallel to the length of the specimen. Then, a 100–200 μm long precrack could be obtained by backcutting the tapered region.

In situ observations of crack propagation were conducted with the applied-moment DCB test stage (Fig. 2a) mounted in the chamber of a field-emission scanning electron microscope (SEM, Hitachi S4100). The prenotched and precracked DCB specimen was attached to the specimen loading arms using an epoxy adhesive, as shown in Fig. 2a. The downward movement of the lower loading arm was controlled by a d.c. drive motor and drive gears. The specimen loading arm was subjected to loading through the loading point pins, and a schematic drawing is shown in Fig. 2b. The total applied load was monitored by a semiconductor load cell, which was attached to the upper loading arm. The crack path was continuously monitored during loading.

In the DCB specimen used here, the layers were parallel to the polished surface of the specimen such that the crack plane and the crack direction were, respectively, normal and parallel to the layers. During the test, the crack plane remained in the groove region initially (when the crack length was less than ~0.5 mm), and then began to deviate from the centreline. However, when the crack reached the edge of the groove, the specimen delaminated along the plane of the bottom surface of the groove, and the crack propagated away from the groove (Fig. 3a). Due to this delamination, the crack did not go through the thickness of the specimen. Instead, the crack propagated only in the layers containing no groove (Fig. 3b). However, the crack turned back towards the groove before it reached the edge of the specimen. This turning-back occurred once or twice before the specimen failed with the crack reaching the end of the specimen in the groove region. A schematic drawing of an S-shaped crack (i.e. a crack with two turning-back points) is shown in Fig. 3a. A cross-section of the DCB specimen is shown schematically in Fig. 3b, where h_0 (= 4.94 mm) and b (= 2.32 mm) are the half-width and the thickness of the specimen, and w (= 0.89 mm) and a (= 1.32 mm) are the half-width and the depth of the groove, respectively.

For the observed S-shaped crack (see Fig. 3a), the deviated crack grew stably until just before the first turn-back. Then, unstable propagation occurred until the crack had just passed the centreline. With increasing load, the crack propagated stably until slightly before the second turn-back. This was then followed by unstable propagation. A schematic drawing of the crack path on the polished surface of the specimen with one and two turn-backs is shown in Fig. 4. The observed stable and unstable crack propagations are indicated by solid and dashed lines, respectively. It is noted that for a non-laminated material, the propagation of a deviated crack is usually unstable and does not turn back. Hence, compared to the propagation of a deviated crack in a non-laminated materials, the propagation of a deviated crack with delamination in a laminated composite is more stable.

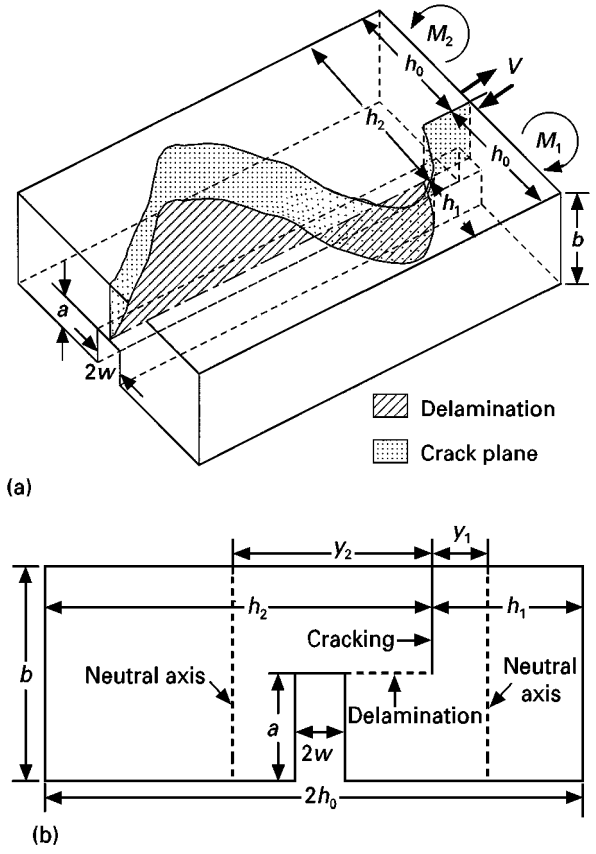

Figure 3 (a) Schematic drawing showing an S-shaped crack. The specimen partially delaminates along the plane of the bottom surface of the groove, and the crack deviates from the groove region during crack propagation. (b) Schematic drawing showing a cross-section of the specimen. Both the partial delamination and the deviated crack are shown.

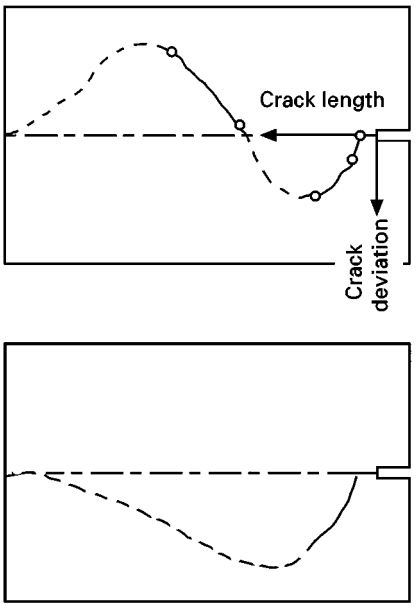

Figure 4 Schematic drawing showing the crack path on the polished surface of the specimen with one and two turn-backs. The (—) stable and (- - -) unstable crack propagation are indicated. (○) Positions for the data measured in Table I.

3. Analyses

When the crack remains in the groove region, the applied stress intensity (i.e. the toughness of the material), K, can be calculated readily from [1]

$$K = \frac{M_0}{[(b-a)\,I_0]^{1/2}} \tag{1}$$

where M_0 is the applied bending moment on each beam, and I_0 is the moment of inertia of the cross-section of the beam (i.e. half of the specimen) with respect to the neutral axis. The bending moment applied on each beam, M_0, equals half the total load multiplied by the distance between the inner and the outer loading pins (Fig. 2a). The moment of inertia of the beam with a groove has been derived, such that [12]

$$I_0 = \frac{bh_0^3 - aw^3}{3} - \frac{(bh_0^2 - aw^2)^2}{4(bh_0 - aw)} \tag{2}$$

When the crack deviates from the groove, the specimen partially delaminates along the plane of the bottom surface of the groove, and the crack propagates in the layers containing no groove. In the presence of asymmetric cracking, the cross-sections of both beams vary along the length direction as the crack propagates (see Fig. 3a). However, it has been proved that a simple beam formula derived for a beam with a uniform cross-section can be used with sufficient accuracy in calculating the normal bending stress in a beam of variable cross-section [13]. Ignoring the variable cross-section of the beam, the cross-section at the crack front is considered in the present study to determine the change of the elastic energy during crack propagation. Also, due to asymmetric cracking, the applied moment induces mixed-mode loading on the specimen [14]. Based on the elastic energy change during crack propagation, the apparent applied stress intensity (and hence the apparent fracture resistance of the specimen) is calculated in the present study.

Assuming that the two beams have widths h_1 and h_2, respectively (see Fig. 3b), these widths satisfy

$$h_1 + h_2 = 2h_0 \tag{3}$$

The moments of inertia of these two beams, I_1 and I_2, become

$$I_1 = \frac{b(h_0 - w)^3 - (b-a)\;(h_0 - h_1 - w)^3}{3} - \frac{[b(h_0 - w)^2 - (b-a)\;(h_0 - h_1 - w)^2]^2}{4[b(h_0 - w) - (b-a)\;(h_0 - h_1 - w)]} \tag{4a}$$

$$I_2 = \frac{bh_2^3 - a(h_0 - h_1 + w)^3}{3} - \frac{[bh_2^2 - a(h_0 - h_1 + w)^2]^2}{4[bh_2 - a(h_0 - h_1 + w)]} \tag{4b}$$

Assuming an equal bending moment, M_0, applied on each beam, the applied stress intensity, K_b, can be related to the applied moment, M_0, by [15]

$$K_b = M_0\left[\frac{1}{2(b-a)\;I_1} + \frac{1}{2(b-a)\,I_2}\right]^{1/2} \tag{5}$$

Combining Equations 1 and 5, the normalized applied stress intensity, K_b/K, is

$$\frac{K_b}{K} = \left[\frac{I_0(I_1 + I_2)}{2I_1I_2}\right]^{1/2} \quad (6)$$

Owing to the asymmetric crack, it is reasonable to assume that the applied load is unevenly distributed such that loads F_1 and F_2, are applied, respectively, at the two outer loading point pins (Fig. 2b). The applied loads satisfy

$$F_1 + F_2 = 2F_0 \quad (7)$$

where $2F_0$ is the total applied load. These applied loads would induce forces R_1 and R_2, at the two inner loading point pins (Fig. 2b). Using the condition of equilibrium of the bending moment, it can be derived that

$$R_1 = F_1 + \frac{(F_1 - F_2)q}{2p} \quad (8a)$$

$$R_2 = F_2 + \frac{(F_2 - F_1)q}{2p} \quad (8b)$$

where p (= 25.4 mm in this case) is the half distance between the two inner loading point pins, and q (= 19 mm in this case) is the distance between the inner and the outer loading point pins.

Based on the forces, F_1, F_2, R_1 and R_2, the applied moments, M_1 and M_2, at the locations of neutral axes of the two beams can be derived, such that

$$M_1 = F_1q + (F_1 - R_1)\,[p - (h_2 - h_0 + y_1)] \quad (9a)$$

$$M_2 = F_2q + (F_2 - R_2)\,[p - (y_2 - h_2 + h_0)] \quad (9b)$$

where y_1 and y_2 are the distance in the specimen width direction from the neutral axes of the two beams, respectively, to the crack front (Fig. 3b). The location of the neutral axis has been derived [12], and y_1 and y_2 are

$$y_1 = \frac{b(h_0 - w)^2 - (b - a)\,(h_0 - h_1 - w)^2}{2[b(h_0 - w) - (b - a)\,(h_0 - h_1 - w)]} - (h_0 - h_1 - w) \quad (10a)$$

$$y_2 = \frac{bh_2^2 - a(h_0 - h_1 + w)^2}{2[bh_2 - a(h_0 - h_1 + w)]} \quad (10b)$$

Substitution of Equations 7 and 8 into Equations 9a and b yields

$$M_1 = F_0q + \frac{(F_1 - F_0)\,q(h_2 - h_0 + y_1)}{p} \quad (11a)$$

$$M_2 = F_0q + \frac{(F_0 - F_1)\,q(y_2 - h_2 + h_0)}{p} \quad (11b)$$

Due to the non-uniform bending moment distribution (i.e. $M_1 \neq M_2$), a shear force, V, is induced, such that V equals the bending moment gradient along the specimen width direction [13]. The average shear force on the specimen is hence

$$V = \frac{M_2 - M_1}{y_1 + y_2} \quad (12)$$

Substitution of Equations 11a and b into Equation 12 yields

$$V = \frac{(F_0 - F_1)q}{p} \quad (13)$$

Whereas the applied bending moments M_1 and M_2, induce a mode I load, the shear force, V, induces a mode II load at the crack tip. The total elastic energy change, dW, during crack propagation is

$$dW = \frac{1}{2E}\left(\frac{M_1^2}{I_1} + \frac{M_2^2}{I_2} + \frac{V^2}{A_1} + \frac{V^2}{A_2}\right)dc \quad (14)$$

where E is Young's modulus of the specimen, c is the crack length, and A_1 and A_2 are the cross-sectional areas of the two beams, respectively, such that (see Fig. 3b)

$$A_1 = b(h_0 - w) - (b - a)\,(h_0 - h_1 - w) \quad (15a)$$

$$A_2 = bh_2 - a(h_0 - h_1 + w) \quad (15b)$$

The corresponding apparent applied stress intensity, K_m, is

$$K_m = \left[\frac{1}{2(b - a)}\left(\frac{M_1^2}{I_1} + \frac{M_2^2}{I_2} + \frac{V^2}{A_1} + \frac{V^2}{A_2}\right)\right]^{1/2} \quad (16)$$

To derive the uneven distribution of the applied load, it is assumed that the total applied load is distributed between the two outer loading point pins in such a way that dW is minimized. Using Equations 11, 13, and 14, the condition of minimum energy change leads to

$$F_1 = F_0 - \frac{pF_0\left(\frac{h_2 - h_0 + y_1}{I_1} - \frac{y_2 - h_2 + h_0}{I_2}\right)}{\left[\frac{(h_2 - h_0 + y_1)^2}{I_1} + \frac{(y_2 - h_2 + h_0)^2}{I_2} + \frac{1}{A_1} + \frac{1}{A_2}\right]} \quad (17)$$

It is noted that the condition of minimum energy change (i.e. Equation 17) can lead to a negative value of R_1 or R_2 when the deviation of h_1 (and hence h_2) from h_0 exceeds a limit. However, based on the loading fixture depicted in Fig. 2, R_1 and R_2 cannot be negative. Hence, a constraint exists for Equation 17 to ensure non-negative values for R_1 and R_2. Using Equations 8a and b, this constraint is

$$\frac{qF_0}{p + q} \leqslant F_1 \leqslant \frac{(2p + q)\;F_0}{p + q} \quad (18)$$

When F_1 in Equation 17 is beyond the range defined by Equation 18, the limiting value in Equation 18 should be used.

4. Results

Assuming $h_1/h_0 = 0.5$, the calculated normalized forces, R_1/F_0 and R_2/F_0, at the two inner loading point

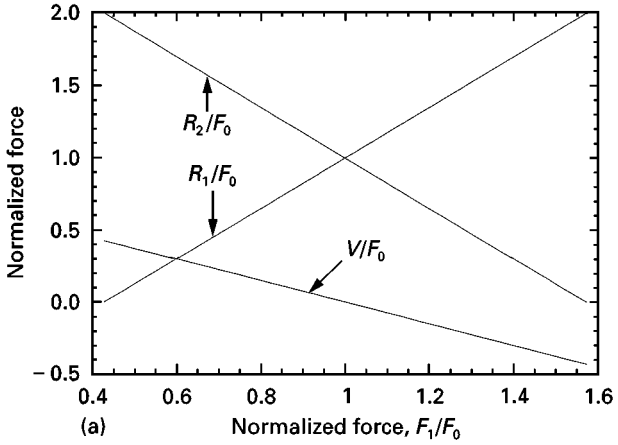

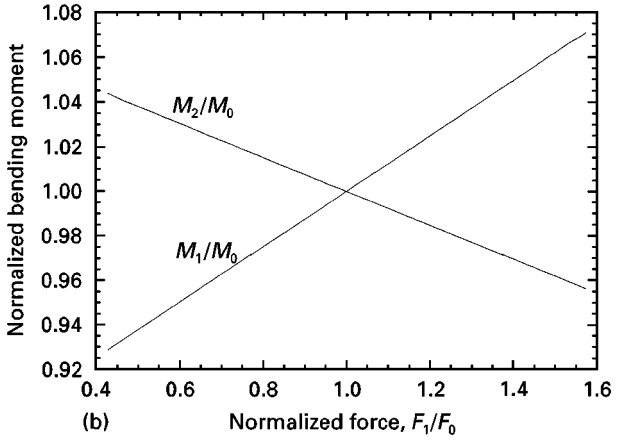

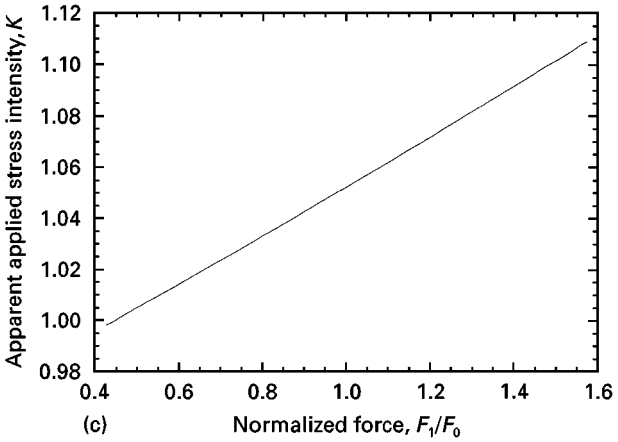

Figure 5 The calculated (a) normalized forces, R_1/F_0, R_2/F_0, and V/F_0, (b) normalized bending moment, M_1/M_0 and M_2/M_0, and (c) normalized apparent applied stress intensity as functions of the normalized applied force, F_1/F_0, for applied-moment DCB tests performed on the Si_3N_4/BN–Al_2O_3 laminate and $h_1/h_0 = 0.5$.

pins, and normalized shear force, V/F_0, on the specimen as functions of the normalized applied force, F_1/F_0, are shown in Fig. 5a. The range of F_1 shown in Fig. 5a satisfies Equation 18. In the case of symmetric loading (i.e. $F_1 = F_2 = F_0$), $R_1 = R_2 = F_0$ and $V = 0$. When F_1/F_0 increases from $q/(p+q)$ to $(2p+q)/(p+q)$, R_1/F_0 increases from 0 to 2, R_2/F_0 decreases from 2 to 0, and V/F_0 decreases from 0.43 to -0.43. The corresponding normalized applied bending moments on the two beams, M_1/M_0 and M_2/M_0, are shown in Fig. 5b where $M_0 = F_0 q$. Asymmetric

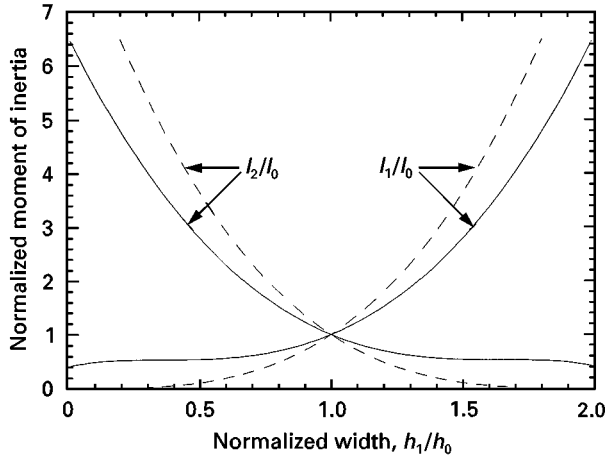

Figure 6 The calculated normalized moments of inertia of the two beams, I_1/I_0 and I_2/I_0, during asymmetric cracking as functions of the normalized width of the beam, h_1/h_0, for applied-moment DCB tests performed on both the Si_3N_4/BN–Al_2O_3 laminate (—) with delamination and PSZ (- - -) without delamination.

bending moments on the two beams are induced by asymmetric loading (i.e. $M_1 \neq M_2$ when $F_1 \neq F_2$). However, the bending moments on the specimen due to the forces, R_1 and R_2, partially compensate the asymmetry in the applied bending moment caused by asymmetric loading, F_1 and F_2. As a result, the asymmetry in the bending moment is far less than the asymmetry in loading [i.e. $|(M_1 - M_0)/M_0| < |(F_1 - F_0)/F_0|$]. Whereas the asymmetry in loading, $(F_1 - F_0)/F_0$, can be as high as 57 %, the asymmetry in the applied moment, $(M_1 - M_0)/M_0$ is only 7 % (Fig. 5b). Based on applied bending moments in Fig. 5b, and the shear force in Fig. 5a, the normalized apparent applied stress intensity as a function of F_1/F_0 is shown in Fig. 5c. The apparent applied stress intensity decreases with the decrease in F_1. It is noted that the loading, F_1 required to give the minimum appparent applied stress intensity (see Equation 17) in this case is beyond the range defined by Equation 18.

Combining Equations 2 and 4, the calculated normalized moments of inertia of the two beams, I_1/I_0 and I_2/I_0, during asymmetric cracking of the Si_3N_4/BN $-$ Al_2O_3 laminate as functions of the normalized width of the beam, h_1/h_0, are shown in Fig. 6. When h_1 approaches zero, I_1 has a finite value. This is due to the presence of delamination in the specimen (see Fig. 3b). Using Equations 4, 10, 11, 15, 17 and 18, the calculated normalized uneven applied moments on the beam, M_1/M_0 and M_2/M_0, as functions of the normalized width of the beam, h_1/h_0, are shown in Fig. 7. When $|(h_1 - h_0)/h_0| \gtrsim 0.05$, the loading, F_1, required to give the minimum apparent applied stress intensity is beyond the range defined by Equation 18, and is limited by the higher and the lower bounds defined in Equation 18. As a result, the slope of the curve in Fig. 7 has an abrupt change. For the case of minimum total elastic energy change, the applied moment on the narrower beam is smaller than the evenly distributed one, M_0 (i.e. $M_1 < M_0$ when $h_1/h_0 < 1$). However, the difference is not significant (e.g. $|(M_1 - M_0)/M_0| < 0.06$).

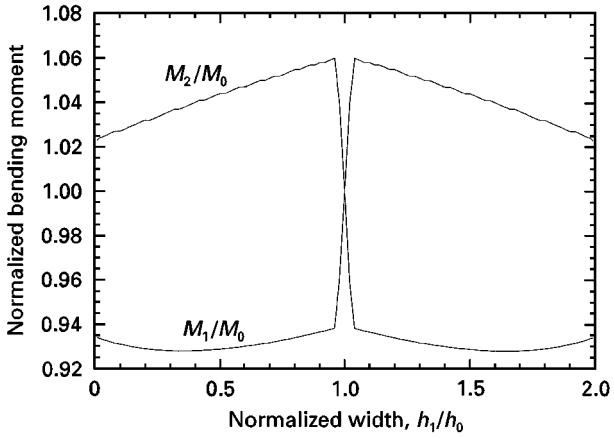

Figure 7 The calculated normalized uneven applied bending moments on the beam, M_1/M_0 and M_2/M_0, as functions of the normalized width of the beam, h_1/h_0, for applied-moment DCB tests performed on the Si_3N_4/BN–Al_2O_3 laminate.

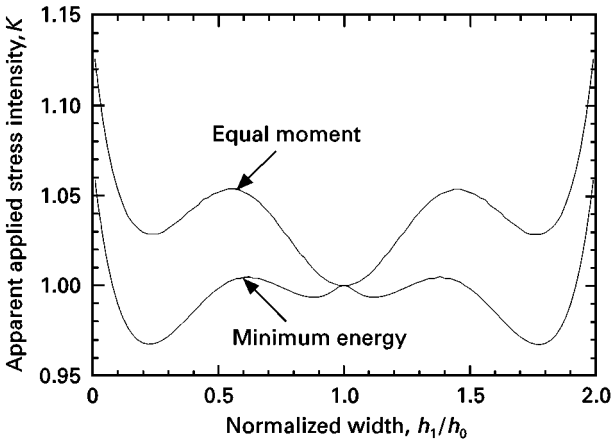

Figure 8 The normalized applied stress intensity as a function of the normalized width of the beam, h_1/h_0, for applied-moment DCB tests performed on the Si_3N_4/BN–Al_2O_3 laminate.

From equations 6 and 16, the normalized apparent applied stress intensity as a function of the normalized width of the beam, h_1/h_0, is shown in Fig. 8. When the applied load remains constant and the applied moment is evenly distributed between the two beams, the applied stress intensity (i.e. K_b) increases initially as the crack deviates from the centreline. Then, K_b decreases slightly when h_1 deviates from h_0 for more than $\sim 0.5\,h_0$, and increases again when h_1 deviates from h_0 for more than $\sim 0.75\,h_0$. If the increase in the fracture resistance of the laminate with respect to the crack length due to the *R*-curve behaviour is smaller than the increase in the applied stress intensity due to crack deviation, crack propagation will be unstable when the deviation of the crack from the centreline is from 0 to $0.5\,h_0$. Crack propagation is stable only when the deviation is from 0.5 to $0.75\,h_0$. This rationale, based on the assumption of equal applied moment on each beam, is in contradiction with the experimental observation of the cracking behaviour.

If the applied bending moment is unevenly distributed between two beams, the applied stress intensity, K_m, is insensitive to the initial crack deviation, and then decreases when the deviation of the crack from the centreline is less than $\sim 0.8\,h_0$ and the applied load remains constant. In this case, stable crack propagation away from the centreline occurs as (i) the fracture resistance of the laminate increases with crack extension, and (ii) the applied stress intensity decreases. On the other hand, crack propagation towards the centreline will be unstable because the applied stress intensity increases when the crack reapproaches the centreline. This rationale agrees with experimental observations.

TABLE I *In situ* measurements of the applied load and the corresponding position of the crack tip during an applied-moment DCB test performed on a Si_3N_4/BN–Al_2O_3 laminate with an S-shaped crack (Fig. 4)

Applied load, F (N)	Crack length C (mm)	Deviation from centreline, (mm)
60	0.365	0
64	2.14	1.338
84	3.552	2.727
86	8.302	− 0.317
103	9.401	− 3.141

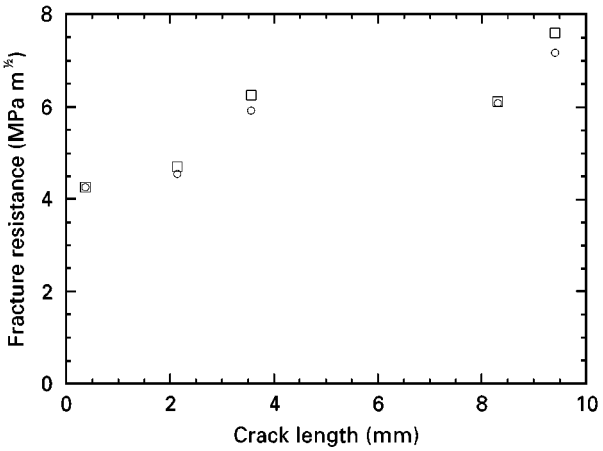

Figure 9 The calculated fracture resistance as a function of the crack length for applied-moment DCB tests performemd on the Si_3N_4/BN–Al_2O_3 laminate. (□) Equal moment, (○) minimum energy.

The steady-state fracture toughness values of Si_3N_4 and 50 % BN–50 % Al_2O_3 layers are, respectively, ~ 3.5 and ~ 2 MPa m$^{1/2}$ [16]. A significant toughening effect is expected for the laminate when both the crack plane and the crack direction are normal to the layers, and the fracture resistance of ~ 12 MPa m$^{1/2}$ has been measured for long crack extensions [16]. On the other hand, the toughening effect is not expected to be as substantial when the crack plane is normal to layers but the crack direction is parallel to layers. Based on *in situ* observations of crack propagation, the measured applied loads and the corresponding positions (i.e. the crack length and the deviation from the centreline) of the crack tip are listed in Table I for an S-shaped crack. Here, the crack length is defined as the distance between the crack tip and the notch tip in the specimen length direction. The positions of the measured crack tip during crack propagation are also indicated by open circles in Fig. 4. Using the data in Table I, the calculated apparent fracture resistance as a function of the crack length is shown in Fig. 9.

Whereas the fracture resistance prediction based on Equation 5 is unreasonable, as discussed above, the prediction based on Equation 16 is more reliable. However, the difference between the two predictions is not significant. For laminates with the crack plane normal to the layers but the crack direction is parallel to the layers, a slight toughening effect is exhibited based on results obtained from Equation 16.

Difficulties exist in explaining the turning-back of the deviated crack (Fig. 4). Owing to the weak interphase of the $BN - Al_2O_3$ layer, the energy required for delamination is not considered in the analysis. Compared to crack propagation towards the centreline, crack propagation away from the centreline induces a greater delamination area. Hence, the turning-back of the deviated crack may be due to delamination, because it is energetically favourable to have a crack propagate towards the centreline when the energy required for delamination is considered.

5. Effects of delamination

To examine the effects of delamination on the stability of the propagation of a deviated crack, applied-moment DCB tests were also performed on non-laminated materials (partial stabilized ZrO_2; i.e. PSZ in this case) with a precrack and a groove machined off the centreline ($h_1/h_0 = 0.5$ and 0.67 in this case) [17]. It is found that the crack propagates towards the beam with a narrower width, becomes unstable, and does not turn back towards the centreline. Considering the PSZ specimen geometry and following the above analytical procedures, the moment of inertia of the beam, the applied moment, and the apparent applied stress intensity can be analysed [17].

The calculated normalized moments of inertia of the two beams, I_1/I_0 and I_2/I_0, of the PSZ specimen as functions of the normalized width of the beam, h_1/h_0, are also shown in Fig. 6. Compared to a deviated crack without delamination, a deviated crack with delamination has a smaller difference between I_1 and I_2 at a fixed h_1/h_0. The normalized apparent applied stress intensity of the PSZ specimen as a function of the normalized width of the beam, h_1/h_0, is shown in Fig. 10. The difference between the results derived from the equal bending moment condition and the minimum energy condition is negligible. The apparent applied stress intensity increases with the increase in the deviation of the crack from the centreline. Hence, if the increase in the fracture resistance of the material with respect to the crack length due to the *R*-curve behaviour is smaller than the increase in the applied stress intensity due to crack deviation, crack propagation will be unstable. Compared to a deviated crack without delamination (Fig. 10), a deviated crack with delamination (Fig. 8) has a much smaller applied stress intensity at a fixed h_1/h_0. Hence, delamination in a laminated composite helps to stabilize the propagation of a deviated crack. The stabilization of a deviated crack with delamination is mainly due to a decrease in the inequality in the moment of inertia of the two beams compared to that without delamination (Fig. 6).

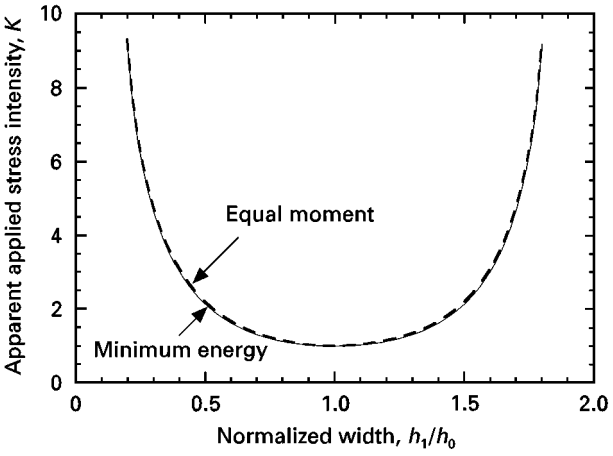

Figure 10 The normalized applied stress intensity as a function of the normalized width of the beam, h_1/h_0, for applied-moment DCB tests performed on PSZ without delamination.

6. Conclusion

In situ observations of crack propagation in an applied moment DCB specimen have been used to obtain the *R*-curve behaviour of Si_3N_4/BN–Al_2O_3 laminated ceramic composites. Owing to weak interphases of the BN–Al_2O_3 layers, the specimen is prepared such that the crack plane and the crack direction are normal and parallel to the layers of the laminate, respectively. Despite a groove along the centreline of the specimen to guide the crack, the specimen partially delaminates along the plane of the bottom surface of the groove, and the crack deviates from the groove region during crack propagation (Fig. 3). However, the crack turns back towards the groove before it reaches the side of the specimen (see Fig. 4). It is found that whereas crack propagation away from the centreline is stable, crack propogation towards the centreline is unstable.

Two approaches were used in the present study to analyse asymmetric cracking in DCB specimens. First, an equal applied moment on both beams is assumed. This assumption leads to the result that crack propagation is unstable when it deviates from the centreline which is in contradiction with experimental observations. Second, the total elastic energy stored in the specimen during crack propagation is assumed to be minimum. This assumption leads to an uneven distribution of applied moment between the two beams when asymmetric cracking occurs (Fig. 7), and the stability of propagation of the asymmetric crack (see Fig. 8) agrees with experimental observations. However, the difference in the *R*-curves obtained by assuming equal applied moment and minimum energy stored in the DCB specimen during crack propagation, is not significant (Fig. 9). Also, despite the fact that the applied forces on the two outer loading point pins (Fig. 2b) can be quite asymmetric, the asymmetry in the applied moment is significantly less (Fig. 5b). This is because the bending moments due to the induced forces at the two inner loading point pins partially compensate the asymmetry in the bending moment caused by asymmetric loading at the two outer loading point pins.

Without delamination, a deviated crack would become unstable due to the increase in the applied stress intensity with the increase in the deviation of the crack from the specimen centreline during the applied moment DCB test (Fig. 10). It was found in the present study that delamination in a laminated composite helps to stabilize the propagation of a deviated crack. The stabilization of a deviated crack with delamination is due to a decrease in the inequality in the moment of inertia of the two beams compared to that without delamination (Fig. 6).

Acknowledgements

The authors thank Drs M. K. Ferber and A. A. Wereszczak for reviewing the manuscript. The research was sponsored by the US Department of Energy, Division of Material Sciences, Office of Basic Energy Sciences, under contract DE-AC05-96OR22464 with Lockheed Martin Energy Research Corp. J.B.L. is also grateful to the National Natural Science Foundation of China for support during his sabbatical.

References

1. S. W. FREIMAN, D. R. MULVILLE and P. W. MAST, *J. Mater. Sci.* **8** (1973) 1527.
2. P. F. BECHER, C. H. HSUEH, K. B. ALEXANDER and E. Y. SUN, *J. Am. Ceram. Soc.* **79** (1996) 298.
3. E. Y. SUN, P. F. BECHER, S. B. WATERS, C. H. HSUEH, K. P. PLUCKNETT and M. J. HOFFMAN, to be published in "Ceramic Microstructures '96: Control at the Atomic Level", edited by A. P. Tomsia and A. Glaeser, (Plenum Press, New York, NY) (1998) p. 779–786.
4. K. P. PLUCKNETT, P. F. BECHER and K. B. ALEXANDER, *J. Microsc.* **185** (1997) 206.
5. M. G. JENKINS, A. S. KOBAYASHI, K. W. WHITE and R. C. BRADT, *J. Am. Ceram. Soc.* **70** (1987) 393.
6. P. F. BECHER, C. H. HSUEH, P. ANGELINI and T. N. TIEGS, *ibid.* **71** (1988) 1050.
7. R. F. KRAUSE, E. R. FULLER and J. F. RHODES, *ibid.* **73** (1990) 559.
8. G. VEKINIS, M. F. ASHBY and P. W. R. BEAUMONT, *Acta Metall. Mater.* **38** (1990) 1151.
9. J. HOMENY and W. L. VAUGHN, *J. Am. Ceram. Soc.* **73** (1990) 2060.
10. T. MIYAJIMA, Y. YAMAUCHI and T OHJI, *Ceram. Trans.* **57** (1995) 425.
11. J. B. LI, unpublished work, 1998.
12. C. H. HSUEH, E. Y. SUN, P. F. BECHER and K. P. PLUCKNETT, *J. Mater. Res.*, submitted, in press (1998).
13. S. P. TIMOSHENKO, "Strength of Materials, Part II: Elementary Theory and Problems", (Van Nostrand, Princeton, N.J., 1956) p. 63.
14. Z. G. SUO and J. W. HUTCHINSON, *Int. J. Solid. struct.* **25** (1989) 1337.
15. H. TADA, P. C. PARIS and G. R. IRWIN, "The Stress Analysis of Cracks Handbook" (Paris Productions, St Louis, Mo, 1985, p. 29.1.
16. P. F. BECHER, unpublished work, (1998).
17. C. H. HSUEH, E. Y. SUN and P. F. BECHER, unpublished work, (1998).

Received 16 June 1997
and accepted 22 April 1998